APPENDIX

A 1 Sample description, sample locations and main foliation

Localities in italic letters are taken from Carta Nazionale della Svizzera, sheet 294, Gressoney (1:50000). All other localities are taken from Carte d´Italia di Instituto Geografico Militare (1:25000), Foglio 42 (Valchiusella, Valprato Soana, Traversella, Pont Canavese, Vistrorio).

Sample	Lithology	Main foliation	Locality	Misc.
MK 1	Metakinzigite (Sill-grt-bt-schist)	245/65	*R 630125 H 68435*	
MK 2	Grt-bearing ep/zo-fsp-wm-schist	206/20	*R 632750 H 78120*	Thin section
MK 3	Ep/zo-fsp-white mica-schist	180/51	*R633125 H 78095*	Thin section
MK 4	Mica-rich chl-ep/zo-fsp-schist	160/61	*R 626750 H 62550*	
MK 5	Grt-bearing bt-chl-ep/zo-fsp-wm-schist	210/05	*R 628955 H 61790*	Thin section
MK 6	Mica-rich chl-ep/zo-fsp-schist	---------	*R 627950 H 62480*	
MK 7	Ep/zo-rich chl-bt-wm-schist	160/60	*R 625750 H 62650*	Thin section
MK 8	cc-bearing ep/zo-rich chl-bt-wm-schist	180/60	*R 625750 H 62650*	Thin section
MK 9	Chl-fsp-bearing calc-schist	125/65	*R 624480 H 62755*	
MK 10	Chl-fsp-bearing calc-schist	112/70	*R 624480 H 62755*	
MK 11	Fine-grained mafic greenschist	95/40	*R 624480 H 62755*	Thin section
MK 12	Mica-rich chl-ep/zo-fsp-schist	125/40	R 394658 H 5041340	Thin section
MK 15	Chl-ep/zo-fsp-schist	60/25	*R 629245 H 66450*	Thin section
MK 16	Bt-chl-bearing ep/zo-white mica-schist	135/35	*R 628800 H 66450*	Thin section
MK 17	Chl-ep/zo-fsp-schist	340/68	*R 628750 H 67150*	Thin section
MK 18	Chl-ep/zo-fsp-schist	275/75	*R 629000 H 67000*	Thin section
MK 19	Chl-ep/zo-fsp-schist	125/58	*R 629000 H 67000*	
MK 20	Qtz-rich chl-white mica-schist	150/80	*R 628650 H 66120*	
MK 21	Qtz-fsp-rich chl-ep/zo-gneiss	---------	*R 628800 H 67750*	Thin section
MK 22	Chl-ep/zo-fsp-schist	---------	*R 629000 H 67450*	Thin section
MK 23	Amph-bearing chl-ep/zo-fsp-schist	180/89	*R 635850 H 66450*	Thin section
MK 24	Grt-ep/zo-white mica-schist	185/89	*R 635850 H 66450*	Thin section
MK 25	Amph-bearing grt-ep/zo-	260/45	R 401810	Thin section

	white mica-schist		H 5051073	Amph-thermometry
MK 26	Ep/zo-white mica-schist	315/38	*R 637350* *H 65780*	Thin section
MK 27	Ep/zo-white mica-schist	315/38	*R 637350* *H 65780*	Thin section
MK 28	Bt-chl-bearing grt-ep/zo-white mica-schist	290/27	*H 635750* *R 66310*	Thin section
MK 29	Chl-bearing ep/zo-white mica-schist	325/89	*H 635750* *R 66310*	
MK 30	Bt-bearing ep/zo-grt-sodic amph-white mica-schist	190/68	R 398665 H 5042887	Thin section
MK 31	Chl-bearing ep/zo-white mica-schist	015/35	R 397073 H 5043352	
MK 32	Qtz-rich grt-bearing white mica-schist	355/89	R 396303 H 5045112	
MK 33	Qtz-rich white mica-schist	345/70	R 396230 H 5045150	
MK 34	Amph-bt-bearing grt-ep/zo-white mica-schist	330/85	R 396674 H 5043201	
MK 35	Amph-bt-bearing grt-ep/zo-white mica-schist	345/65	R 396342 H 5043403	Thin section Forward modelling Amph-thermometry
MK 36	Qtz-rich grt-bearing white mica-schist	025/25	R 399182 H 5043507	Thin section
MK 37	Ep/zo-fsp-white mica-schist	078/30	R 391312 H 5046015	
MK 38	Fine-grained fsp-rich white-mica-schist	078/30	R 391312 H 5046015	Thin section
MK 39	Fine-grained chl-bt-white-mica-schist	142/35	R 383250 H 5044250	Thin section
MK 40	Qtz-rich chl-white-mica calc-schist	145/40	R 388050 H 5037050	Thin section
MK 41	Qtz-rich chl-white-mica calc-schist	075/42	R 388050 H 5037050	Thin section
MK 42	Qtz-rich grt-bearing omph-white mica-schist	325/74	R 399126 H 5042190	Thin section
MK 50	Bt-bearing ep/zo-grt-sodic amph-white mica-schist	355/69	R 397225 H 5042986	
MK 51	Bt-bearing ep/zo-grt-sodic amph-white mica-schist	---------	R 396392 H 5043395	Thin section
MK 52	Amph-bearing grt-sodic amph-white mica gneiss	345/80	R 396392 H 5043395	Thin section Amph-thermometry
MK 53	Amph-bt-bearing grt-ep/zo-white mica-schist	330/60 FAP2	R 396392 H 5043395	Thin section
MK 54	Chl-bearing ep/zo-white mica-schist	345/70	R 394839 H 5044772	Thin section
MK 55	Omph-bearing ep/zo-grt-sodic amph-white mica-schist	200/30	R 399314 H 5042265	Thin section Forward modelling
MK 56	Bt-bearing ep/zo-grt-sodic amph-white mica-schist	072/30	R 402507 H 5040895	
MK 57	Grt-omph-bearing mafic blueschist	330/60 FAP2	R 396392 H 5043395	Thin section
MK 58	Grt-omph-bearing mafic blueschist	325/87	R 403289 H 5048842	Thin section
MK 59	Bt-bearing ep/zo-grt-sodic amph-white mica-schist	327/80	R 403289 H 5048842	Thin section
MK 60	Amph-bt-bearing grt-ep/zo-white mica-schist	015/57	R 401182 H 5048639	Thin section
MK 61	Grt-ep/zo-sodic amph-white mica-schist	250/70	R 406788 H 5052836	

MK 62	Omph-bearing ep/zo-grt-sodic amph-white mica-schist	220/60	R 406866 H 5052557	Thin section
MK 63	Qtz-rich ep/zo-chl-white mica schist	140/70	R 398555 H 5056427	Thin section
MK 64	Chl-ep/zo-white mica-schist	165/68	R 397451 H 5050193	Thin section
MK 65	Qtz-rich ep/zo-chl-white mica schist	---------	R 396907 H 5049512	
MK 70	Grt-omph-bearing mafic blueschist	280/15	R 409599 H 5058632	
MK 71	Grt-ep/zo-sodic amph-white mica-schist	010/35 FAP3	R 409727 H 5058599	Thin section
MK 72	Grt-ep/zo-white mica-schist	355/25	R 406878 H 5048820	Thin section
MK 73	Grt-bearing ep/zo-white mica-schist	358/40	R 406740 H 5049093	Thin section
MK 74	Chl-ep/zo-fsp-schist	152/80	R 402628 H 5051604	Thin section
MK 75	Amph-bearing qtz-rich chl-white mica-schist	340/65	R 402489 H 5051967	
MK 76	Qtz-rich ep/zo-chl-white mica schist	310/60	R 402489 H 5051967	
MK 77	Fine grained ep/zo-rich mafic greenschist	152/70	R 402289 H 5053430	Thin section
MK 78	Ep/zo-fsp-white mica-schist	130/75	R 402159 H 5053477	
MK 79	Qtz-rich ep/zo-chl-white mica schist	130/70	R 402159 H 5053477	Thin section
MK 80	Amph-bearing qtz-rich chl-white mica-schist	140/80	R 401815 H 5053700	Thin section Amph-thermometry
MK 81	Qtz-rich ep/zo-white mica-fsp-schist	155/85	R 399436 H 5052652	Thin section
MK 82	Qtz-rich ep/zo-chl-white mica schist	148/80	R 399236 H 5052628	
MK 83	Chl-fsp-bearing calc-schist	135/82	R 394658 H 5050240	
MK 84	Qtz-rich cc-bearing chl-ep/zo-fsp-schist	342/80	R 395398 H 5050187	
MK 85	Ep/zo-fsp-white mica-schist	132/55	R 403752 H 5062154	Thin section
MK 86	Chl-fsp-bearing calc-schist	130/50	R 402908 H 5062269	
MK 87	Chl-fsp-bearing calc-schist	115/60	R 405216 H 506529	
MK 88	Qtz-rich ep/zo-chl-white mica schist	126/50	R 398569 H 5055347	
MK 89	Amph-bt-bearing grt-ep/zo-white mica-schist	126/47	R 398569 H 5055347	
MK 90	Bt-bearing ep/zo-white mica-schist	140/78	R 399661 H 5054338	
MK 91	Ep/zo-fsp-white mica-schist	122/65	R 399703 H 5054314	
MK 92	Ep/zo-fsp-white mica-schist	132/55	R 399703 H 5054314	Thin section Amph-thermometry
MK 93	Ep/zo-fsp-white mica-schist	---------	R 399703 H 5054314	
MK 94	Bt-bearing ep/zo-white mica-schist	142/89	R 401097 H 5052262	Thin section
MK 95	Chl-bearing Bt-ep/zo-white mica-schist	150/89	R 401097 H 5052262	Thin section

MK 96	Chl-bearing Bt-ep/zo-white mica-schist	135/89	R 401097 H 5052262	
MK 97	Amph-bearing grt-ep/zo-white mica-schist	325/50	R 406111 H 5055426	Thin section
MK 98	Grt-ep/zo-white mica-schist	---------	R 405762 H 5056057	Thin section
MK 99	Grt-sodic amph-ep/zo-white mica-schist	342/87	R 405762 H 5056057	Thin section
MK 100	Chl-bearing ep/zo-fsp-white mica-schist	292/80	R 402732 H 5054652	Thin section
MK 101	Qtz-rich ep/zo-chl-white mica schist	250/27	R 403446 H 5054550	
MK 102	Qtz-rich ep/zo-chl-white mica schist	322/75	R 403446 H 5054550	
MK 104	Ep/zo-fsp-white mica-schist	114/86	R 402840 H 5054650	Thin section
MK 105	Grt-bearing chl-bt-ep/zo-white mica-schist	350/50	R 402648 H 5054719	Thin section
MK 106	Grt-bearing chl-bt-ep/zo-white mica-schist	300/60	R 402648 H 5054719	
MK 107	Grt-bearing chl-bt-ep/zo-white mica-schist	300/75	R 402648 H 5054719	
MK 109	Chl-ep/zo-white mica-schist	184/35	R 402706 H 5054705	
MK 110	Bt-amph-ep/zo-white mica-schist	140/60	R 401459 H 5054557	Thin section Amph-thermometry
MK 111	Chl-ep/zo-white mica-schist	130/50	R 401530 H 5054531	
MK 112	Amph-bearing qtz-rich chl-white mica-schist	140/40	R 401847 H 5054743	
MK 113	Ep/zo-fsp-white mica-schist	130/60	R 401889 H 5054717	
MK 114	Ep/zo-fsp-white mica-schist	---------	R 401889 H 5054717	
MK 115	Ep/zo-fsp-white mica-schist	172/47	R 401889 H 5054717	
MK 116	Chl-ep/zo-white mica-schist	160/45	R 401858 H 5054774	Thin section
MK 117	Chl-bearing grt-sodic amph-white mica-schist	180/55	R 406169 H 5055159	Thin section Forward modelling
MK 118	Cc-bearing grt-chl-ep/zo-sodic amph-white mica-schist	322/60	R 406150 H 5055641	Thin section
MK 119	Qtz-rich ep/zo-chl-white mica schist	190/55	R 409797 H 5058347	
MK 120	Sodic amph-bearing grt-ep/zo-amph-mica-schist	154/60	R 407772 H 5057769	Thin section
MK 121	Sodic amph-bearing grt-ep/zo-amph-mica-schist	152/60	R 407772 H 5057769	Thin section
MK 122	Mica-rich chl-ep/zo-fsp-mica-schist	088/46	R 407419 H 5065619	Thin section
MK 123	Chl-ep/zo-fsp-schist	252/65	R 402489 H 5051967	
MK 124	Chl-ep/zo-fsp-schist	320/82	R 402489 H 5051967	
MK 125	Chl-bearing ep/zo-fsp-white mica-schist	177/28	R 403237 H 5058553	Thin section
MK 126	Bt-bearing ep/zo-grt-sodic amph-white mica-schist	340/20	R 411913 H 5051073	Thin section
MK 127	Bt-bearing ep/zo-grt-sodic amph-white mica-schist	337/80	R 412427 H 5050288	

MK 128	Mica-rich chl-ep/zo-fsp-mica-schist	088/72	R 406123 H 5055725	
MK 129	Mica-rich chl-ep/zo-fsp-mica-schist	327/80	R 406117 H 5055752	Thin section
MK 130	Grt-sodic amph-ep/zo-white mica-schist	166/44	R 406189 H 5055878	Thin section
MK 131	Bt-bearing grt-ep/zo-white mica-schist	184/17	R 406594 H 5055763	Thin section
MK 132	Mica-rich chl-ep/zo-fsp-mica-schist	---------	R 406368 H 5054904	
MK 133	Qtz-white mica-bearing retrogressed eclogite	348/65	R 406230 H 5054699	Thin section
MK 134	Grt-sodic amph-ep/zo-white mica-schist	005/69	R 415664 H 5048995	
MK 136	Bt-bearing grt-ep/zo-white mica-schist	100/20	R 407533 H 5063687	
MK 137	Bt-bearing grt-ep/zo-white mica-schist	100/22	R 407533 H 5063687	Thin section
MK 138	Fsp-rich chl-bt-white mica-schist	122/71	R 388465 H 5038802	
MK 139	Sodic amph-bearing grt-ep/zo-white mica-schist	128/67	R 388527 H 5038874	
MK 140	Sodic amph-bearing grt-ep/zo-white mica-schist	124/50	R 388594 H 5038913	
MK 142	Bt-bearing ep/zo-grt-sodic amph-white mica-schist	085/26	R 401303 H 5040780	
MK 143	Bt-bearing ep/zo-grt-sodic amph-white mica-schist	085/26	R 401303 H 5040780	
MK 150	Grt-bearing chl-ep/zo-gneiss	137/89	R 394928 H 5044605	Thin section
MK 151	Ep/zo-grt-white mica-schist	295/76	R 394928 H 5044605	Thin section
MK 152	Qtz-white mica-bearing grt-ep/zo-blueschist	---------	R 395676 H 5043722	Thin section
MK 153	Bt-bearing ep/zo-grt-sodic amph-white mica-schist	008/50	R 398905 H 5042466	Thin section
MK 154	Ep/zo-white mica-schist	332/20	R 395476 H 5043652	Thin section
MK 154b	Grt-bearing ep/zo-white mica-schist	---------	R 398905 H 5042466	
MK 155	Ep/zo-white mica-schist	332/20	R 395476 H 5043652	Thin section
MK 156	White.mica-bearing marble	---------	R 395221 H 5043361	
MK 157	Qtz-rich ep/zo-chl-white mica schist	020/40	R 394165 H 5045574	Thin section
MK 158	Qtz-rich ep/zo-chl-white mica schist	024/30	R 394185 H 5045577	Thin section
MK 159	Bt-bearing ep/zo-grt-sodic amph-white mica-schist	078/18	R 401415 H 5040977	
MK 160	Grt-bearing ep/zo-white mica-schist	070/15	R 401347 H 5040989	Thin section
MK 161	Grt-bearing ep/zo-white mica-schist	---------	R 401347 H 5040989	
MK 162	Bt-bearing ep/zo-grt-sodic amph-white mica-schist	045/15	R 400878 H 5041245	Thin section Amph-thermometry
MK 163	Ep/zo-grt-omph-sodic amph-white mica-schist	020/30	R 400878 H 5041245	Thin section Forward modelling
MK 166	Grt-bearing bt-sodic amph-white mica-schist	080/55	R 398754 H 5032954	

MK 167	Grt-bearing bt-sodic amph-white mica-schist	088/57	R 399256 H 5033125	
MK 168	Grt-bearing bt-sodic amph-white mica-schist	072/42	R 401005 H 5033410	Thin section
MK 169	Grt-bearing bt-sodic amph-white mica-schist	152/47	R 401750 H 5033620	Thin section
MK 170	Bt-bearing ep/zo-grt-white mica-schist	350/36	R 396328 H 5043413	Thin section
MK 171	White-mica bearing qtz-fsp-gneiss	002/85	R 399056 H 5044673	Thin section
MK 172	Ep/zo-grt-omph-sodic amph-white mica-schist	358/72	R 399136 H 5044692	Thin section
MK 173	Ep/zo-grt-omph-sodic amph-white mica-schist	010/37 FAP3	Bio (see map)	
MK 174	Chl-bearing grt-ep/zo-white mica gneiss	340/65	R 394667 H 5044854	Thin section
MK 175	Amph-bearing grt-sodic amph-white mica gneiss	302/57	R 394999 H 5044463	
MK 176	Grt-ep/zo-white mica-schist	302/50	R 394999 H 5044463	Thin section
MK 177	Amph-bearing grt-sodic amph-white mica gneiss	302/17	R 394999 H 5044463	
MK 178	Amph-bearing grt-sodic amph-white mica gneiss	162/79	R 396342 H 5043403	
MK 179	Grt-ep/zo-white mica-schist	350/85	R 406060 H 5053957	Thin section
MK 180	Ep/zo-grt-white mica-schist	310/60	R 406089 H 5053842	Thin section
MK 181	Qtz-rich ep/zo-chl-white mica schist	355/87	R 401452 H 5051641	
MK 182	Chl-fsp-bearing calc-schist	125/70	R 390061 H 5046909	
MK 183	Grt-chl-ep/zo-sodic amph-white mica-schist	038/43	R 402914 H 5045013	Thin section
MK 184	Strongly retrogressed sodic amph-bearing eclogite	---------	R 402715 H 5044889	
MK 185	Qtz-rich grt-sodic amph-white mica-schist	---------	R 402715 H 5044889	
MK 186	Chl-ep-white mica-schist	140/74	R 406735 H 5048986	
MK 187	Chl-ep-white mica-schist	140/74	R 406735 H 5048986	
MK 188	Amph-omph-bearing grt-sodic amph-white mica gneiss	---------	R 396392 H 5043395	
MK 190	Amph-omph-bearing grt-sodic amph-white mica gneiss	---------	R 396392 H 5043395	Thin section
MK 191	Amph-omph-bearing grt-sodic amph-white mica gneiss	---------	R 396392 H 5043395	
MK 192	Chl-cc-white mica-schist	064/34	R 392734 H 5045848	Thin section
MK 193	Chl-fsp-bearing calc-schist	320/76	R 401807 H 5059154	
MK 194	Chl-ep-white mica-schist	135/43	R 402090 H 5058823	
MK 195	Ep/zo-grt-sodic amph-white mica-schist	308/89	R 404975 H 5046578	Thin section
MK 196	Chl-ep-white mica-schist	082/14	R 405001	Thin section

			H 5046690	
MK 197	Grt-omph-white mica schist	035/26	R 404997 H 5046737	
MK 198	Grt-omph-white mica schist	330/57	R 405000 H 5046760	Thin section
MK 199	Chl-bearing amph-ep/zo-white mica-schist	318/81	R 405000 H 5046760	Thin section
MK 200	Monomineralic white mica sample	358/65	R 404978 H 5046752	Thin section
MK 201	Grt-omph-bearing mafic blueschist	280/89	R 404959 H 5046734	Thin section
MK 202	Grt-omph-bearing mafic blueschist	280/89	R 404959 H 5046734	Thin section
MK 203	Grt-bearing ep/zo-white mica-gneiss	280/89	R 404959 H 5046734	Thin section
MK 204	White-mica bearing qtz-fsp-gneiss	280/89	R 404959 H 5046734	Thin section
MK 205	Grt-omph-sodic amph-white mica-schist	352/32 FAP1	R 397300 H 5045085	Thin section
MK 206	Grt-bearing chl-amph-bt-ep/zo-white mica-schist	041/34	R 397300 H 5045085	Thin section Amph-thermometry
MK 207	Grt-bearing chl-amph-bt-ep/zo-white mica-schist	045/50	R 397300 H 5045085	Thin section Amph-thermometry
MK 208	Grt-bearing omph-chl-sodic amph-ep/zo-amph-white mica-schist	---------	R 397233 H 5054232	Thin section Forward modelling Amph-thermometry
MK 209	Qtz-rich grt-sodic amph-white mica-schist	310/60	R 394999 H 5044463	
MK 210	Qtz-rich grt-sodic amph-bearing white mica-schist	312/55	R 394999 H 5044463	
MK 211	Grt-ep/zo-white mica-schist	312/55	R 394999 H 5044463	Thin section
MK 212	Ep/zo-bearing white mica-schist	170/80 FAP2	R 394978 H 5044519	Thin section
MK 213	Ep/zo-white mica-fsp-schist	167/24	R 405150 H 5055841	Thin section
MK 214	Amph-bearing ep/zo-white mica-fsp-schist	037/37	Montestrutto	Thin section
MK 215	Ep/zo-white mica-fsp-schist	164/85	R 394492 H 5045269	Thin section
MK 216	Amph-bearing ep/zo-white mica-fsp-schist	135/48	R 394492 H 5045269	
MK 217	Ep/zo-white mica-fsp-schist	088/60	R 394172 H 5045232	
MK 541	Bt-bearing ep/zo-grt-sodic amph-white mica-schist	165/45	R 399317 H 5042237	

A 2 Analytical procedure

Microprobe analyses were carried out at the Museum of Natural History of the Humboldt University, Berlin with a JEOL 8800 Superprobe, 15 kV acceleration voltage and a beam current of 15 nA. For calibration we used natural standard materials (see below). For post-analytical correction we used the ZAF algorithm. Site occupancies in amphiboles were calculated according to the suggestion of Leake et al., 1997, white mica and chlorite composition was calculated after Vidal and Parra (2000).

Microprobe Measurement Conditions

Crystals used in the wavelength dispersive spectrometers:

Si	**Al**	**Fe**	**Mg**	**Ca**	**Mn**
TAP	TAP	LiF	TAP	PET	LiF

Na	**K**	**Ti**	**Ba**	**Cr**
TAP	PET	LiF	LiF	LiF

Garnet:

Beam diameter: 1µm

Counting time: 20/10 s peak/background for all elements

Measured elements: Si, Al, Fe, Mg, Ca, Mn

Standard materials:

Si	**Al**	**Fe**	**Mg**	**Ca**	**Mn**
Pyrope	Pyrope	Almandine	Almandine	Cr-Augite	Ilmenite

Amphibole:

Beam diameter: 5µm

Counting time: 20/10 s peak/background for main elements

40/20 s peak/background for Cr

Measured elements: Si, Al, Fe, Mg, Ca, Mn, Na, K, Ti, (Cr)

Standard materials:

Si	**Al**	**Fe**	**Mg**	**Ca**	**Mn**
Hypersthen	Albite	Cr-Augite	Cr-Augite	Cr-Augite	Ilmenite

Na	**K**	**Ti**	**Cr**
Albite	Microcline	Ilmenite	Cromite

Mica:

Beam diameter: 5µm

Counting time: 20/10 s peak/background for all elements

Measured elements: Si, Al, Fe, Mg, Ca, Mn, Na, K, Ti

Standard materials:

Si	**Al**	**Fe**	**Mg**	**Ca**	**Mn**
Albite	Albite	Cr-Augite	Cr-Augite	Plagioclase	Ilmenite

Na	**K**	**Ti**
Albite	Microcline	Ilmenite

Feldspar:

Beam diameter: 5µm

Counting time: 20/10 s peak/background for main elements

40/20 s peak/background for Ba

Measured elements: Si, Al, Fe, Mg, Ca, Mn, Na, K, Ti, (Ba)

Standard materials:

Si	Al	Fe	Mg	Ca	Mn
Albite	Albite	Cr-Augite	Cr-Augite	Plagioclase	Ilmenite

Na	K	Ti	Ba
Albite	Microcline	Ilmenite	Benitoite

Epidote:

Beam diameter: 1µm

Counting time: 20/10 s peak/background for all elements

Measured elements: Si, Al, Fe, Mg, Ca, Mn, Na, K, Ti

Standard materials:

Si	Al	Fe	Mg	Ca	Mn
Pyrope	Pyrope	Cr-Augite	Cr-Augite	Cr-Augite	Ilmenite

Na	K	Ti
Albite	Microcline	Ilmenite

Whole rock chemistry

Whole rock chemistry was determined by XRF analysis using an X-ray fluorescence spectrometer at the Museum of Natural History of the Humboldt University, Berlin. The laboratory at the Humboldt University Berlin is equipped with a SIEMENS SRS 3000 wavelength dispersive XRF spectrometer. All analyses are made on fused glass discs prepared from dried and ignited powdered samples. Elements determined as weight % oxide are SiO2, TiO2, Al2O3, Fe2O3(total), MnO, MgO, CaO, Na2O, K2O, and P2O5. Fluid content of the sample is determined by loss on ignition (LOI). Trace elements determined on reconnaissance basis at the> 50 ppm level are V, Cr, Ni, Cu, Zn, Rb, Sr, Y, Zr, Nb, Mo, Sn, Ba, La, and Ce.

A 3 Appendix for Chapter 3

Solid solution models used in Chapter 3:

See Appendix A 5.3

A 4 Appendix for Chapter 4

A 4.1 Historical terminology

In all previous work, a classical subdivision of the Sesia Zone was adopted in which lithologies were defined by a combination of metamorphic criteria (greenschist-, amphibolite-, blueschist-, and eclogite-facies mineral assemblages) and primary lithological features (composition and grain size). This lead to mistaking large retrograde shear zones for primary lithotectonic units, and generally resulted in a confusing nomenclature. A case in point are the frequently used terms “micaschisti eclogitici” and “gneiss minuti”. Originally, these were field mapping terms (e.g. Dal Piaz et al., 1972; Compagnoni et al., 1977, and references therein), but later they were used to define areas in which the rocks preserve distinct Alpine metamorphic conditions. For example, in many papers the term “Gneiss Minuti” is used to refer to all rocks that underwent pervasive retrograde greenschist-facies metamorphism (e.g. Dal Piaz et al., 1972). This is misleading from a geodynamic and structural standpoint, because at least three phases of deformation occurred under retrograde greenschist-facies conditions, as shown in Babist et al., Chapter 4. We note that although some previous workers published evidence for a similar sequence of events as proposed above, none of this previous work covered the entire Sesia Zone.

Several structural and petrological studies present evidence for tectonic contacts between (Williams and Compagnoni 1983) and within rocks units termed “gneiss minuti” and “micaschisti eclogitici” (Pognante 1989a, Passchier et al. 1981). Here, we use the Mesozoic metasediments and metabasic rocks of the Bonze Unit to define the nappe contact between the Bard and Mombarone Units. Our structural investigations have shown that the juxtaposition of the two nappes occurred early, probably during D_1 deformation, as described in Chapter 4. Our deformational phases D_2 and D_3 can be correlated with D_2 and D_3 of Gosso (1977) and the ‘early’ and ‘late postnappe folding’ of Gosso et al. (1979), respectively. Our D_3 phase corresponds to D_5 of Zucali et al. (2002). Our latest ductile deformation phase, D_5 is related to late-orogenic backfolding and backthusting along the Periadriatic Fault System (PFS) in front of the southern Alpine indenter (Schmid et al. 1987, Schmid et al. 1989, Handy et al. 2005).

A 4.2 Appendix geochronology

Sample description:

Sample MK52 is a white-mica bearing sodic-amphibole garnet gneiss from a steeply NNW-dipping S2 shear zone in Val Chiusella (sample coordinates H: 5043395; R: 396392 in a Gauss-Boaga net). Sodic amphibole, phengite and garnet ($Prp_{5.6}$,Alm_{64},Grs_{30}) document blueschist facies conditions. Sodic amphibole is zoned, with barroisitic amphibole at the rim. The barrosite content is estimated to be less than 1 %. Both coarse and fine-grained white mica, as well as Na-amphibole are oriented parallel to S_2. Fe and Mg contents increase at the rims of the amphiboles and fine-grained white mica. These features indicate that the amphiboles and fine-grained white mica grew during D_2. The Rb and Sr concentrations and isotopic compositions are given in Table A 4.1.

Sample RH 1 is from the fine-grained andesitic dyke pictured in Figure 4.8. Ca-amphibole and plagioclase in this sample show magmatic features and contain no traces of deformation. In thin section, magmatic epidote and secondary calcite are present in a statically recrystallised matrix that is interpreted to have been a quenched melt. Epidote and plagioclase with oscillatory zoning both form 1 - 5 mm long phenocrysts. Epidote has corroded grain boundaries. Smaller plagioclase laths with polysynthetic twins occur interstitially. Magmatic Ca-amphibole is also found in the matrix. Accessory minerals are titanomagnetite and, very rarely, pyrite. The secondary calcite is interpreted to be an alteration product, so we focussed on determining the degree of alteration from an isotopic standpoint. To do this, the whole rock was leached with chloro-acetic acid to dissolve the calcite. The concentration of Rb and Sr, as well as the isotopic composition of the insoluble residual (WR – cc) were also determined. All other minerals were treated with the same procedure described above. The results are given in Table A 4.1.

Sample preparation:

Both samples (MK 52 and RH 1) were crushed and sieved, minerals from the sieved fractions were separated by conventional techniques (magnetic separation, heavy liquids, and hand picking). The minerals were dissolved in a mixture (4:1) of hydrofluoric and nitric acid over five days. After drying, the samples were diluted in hydrochloric acid (2.5 M) and divided into two aliquots, one for measuring the isotopic composition and the other for determining the concentration of Sr and Rb by adding spike solutions of both elements. After separating Sr from Rb with ion chromatographic columns, the isotopic composition and the concentration were determined in a mass spectrometer (Finnigan MAT 261). During the analysis, the $^{87}Sr/^{86}Sr$ of a standard (NBS 987) was measured at 0.71026 ± 4 (2σ; n = 12). The standard error of the concentration was estimated to be smaller than 0.4%. Errors of the ratios are given in Table A 4.1.

Table A 4.1: Rb and Sr concentration and Sr isotope composition of the sample MK52 and RH1 and their minerals

Sample	description	Rb ppm	Sr ppm	$^{87}Rb/^{86}Sr$	± 2σ	$^{87}Sr/^{86}Sr$	± σ_m
MK 52	feldspar	2.464	14.53	0.4908	4	0.714677	18
	white mica	117.2	73.10	4.635	42	0.718452	15
RH 1	andesitic dyke (WR)	72.12	882.2	0.2365	21	0.708022	52
	WR – cc*	32.41	557.6	0.1682	15	0.707907	13
	calcite*	1.9527	442.7	0.01276	12	0.708523	17
	plagioclase	200.5	849.0	0.6832	61	0.708092	17
	amphibole	1.578	603.5	0.007565	68	0.707668	16
	epidote	2885	1.988	0.001993	18	0.707748	18

* $C_2H_3O_2Cl$-leachate

Results and Interpretation

Sample MK 52

Coexisting plagioclase and white mica from sample MK 52 yield an age of 63.6 ± 0.8 Ma (Fig. A 4.1). We interpret this to be a formational age for the coarse-grained mica aligned parallel to S_2. This is a maximum age of D_2 deformation because, despite our efforts to separate the grain size fractions carefully, we cannot preclude the possibility that some fine-grained mica remained in the coarse-grained mica fraction.

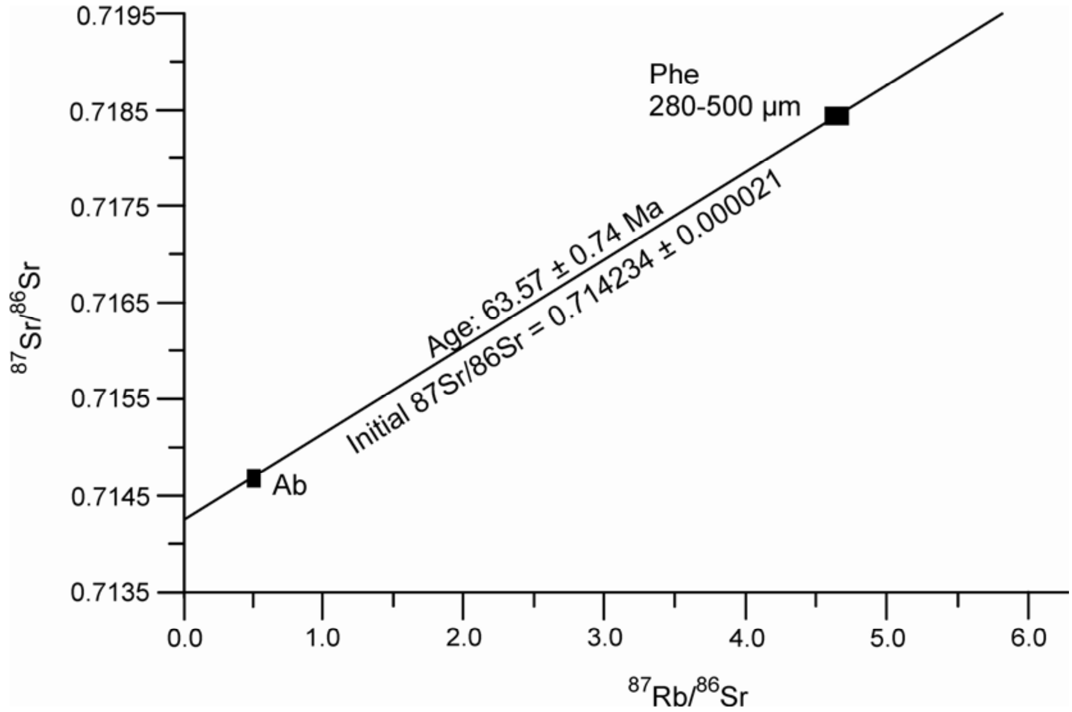

Figure A-1: Rb-Sr isochron diagram of a white-mica bearing sodic-amphibole garnet gneiss from a steeply NNW-dipping S2 shear zone in Val Chiusella (sample MK 52). Ab = albite, Phe = phengite. The slope of the line between albite and phengite defines an age of 63.57 ±0.74 Ma with an initial Sr ratio of 0.714234 ± 0.000021.

Sample RH 1 (see Chapter 4, Fig. 4.8)

All minerals and the whole rock of sample RH 1 have $^{87}Sr/^{86}Sr$ ratios between 0.7077 and 0.7080. However, calcite has a very high $^{87}Sr/^{86}Sr$ ratio (0.7085) despite its very low Rb content (1.95 ppm), indicating that this radionuclide did not contribute to the high $^{87}Sr/^{86}Sr$ ratio. Such a high ratio could not be generated by alteration of the whole rock. Therefore, the Sr source must be external to the rock. Seawater is not a likely source, because the $^{87}Sr/^{86}Sr$ ratio of seawater in Eocene time was determined to be 0.7077. Only in Miocene time did the Sr ratio increase to 0.7085. The most likely source of Sr with a high ratio seems to be continental crust, which liberated a fluid during HP metamorphism due to subduction.

WR – cc has a lower $^{87}Sr/^{86}Sr$ ratio than the whole-rock sample, in agreement with the leached out calcite. An age of 44.2 ± 2.4 Ma was calculated from the slope of the line connecting plagioclase and amphibole. The $^{87}Sr/^{86}Sr$ ratio of the magmatic epidote falls above this line. We cannot exclude the possibility that calcite, epidote and amphibole contributed Sr. Therefore, we interpret the calculated age to be a minimum age for the emplacement of the dyke.

A 5 Appendix for Chapter 5

A 5.1 Rheological models of the upper plate lithosphere (Fig. 5.15)

Viscous shear stress (dashed curves in Fig. 5.15) was estimated by extrapolating experimentally derived constitutive relations for creep (below) to a uniform natural shear strain rate:

$$\dot{\gamma} = \sqrt{3}^{(n+1)} A \cdot e^{(\frac{-H}{R \cdot T})} \cdot \tau^{n} \cdot d^{-m}$$

where $\dot{\gamma}$ is the shear strain rate (assumed here to be 10^{-14} s^{-1}), T is the temperature, τ is the shear stress, and d is the average syntectonic grain diameter (only relevant for Fig. 5.15c, 50 µm). A, H, n and m are material constants for the minerals (olivine, feldspar, quartz) assumed to govern the rheologies, respectively, of the upper mantle, lower crust and intermediate to upper crust of the upper Apulian plate (references for parameters in the figure caption). The rheology was approximated by the following combinations of creep mechanisms and hydrous conditions: dislocation creep of nominally anhydrous or "dry" lithosphere (Fig. 5.15a), dislocation creep of naturally hydrous or "wet" lithosphere (Fig. 5.15b), and viscous granular flow (diffusion-accommodated grain-boundary sliding) of dry lithosphere (Fig. 5.15c). The effect of water in the "wet" examples is restricted to hydrolytic weakening of stoichiometrically anhydrous silicate minerals ("hydrolytic weakening", e.g., Hirth et al. 2001). In all cases, shear stress is limited by frictional sliding on existing fault surfaces at hydrostatic pore-fluid pressure (thick solid curves in Fig. 5.15, regime 3 of Byerlee 1978).

The temperature of deforming rocks surrounding the exhuming Sesia rock body was calculated for a slab-parallel geothermal gradient derived from the P-T path (Fig. 5.13) in this study (shear stress curves labelled "this study" in Fig. 5.15). For comparison, shear stress curves were also calculated for slab-parallel geothermal gradients from a rapidly subducting slab (5cm/a, Nankai slab) and a slowly subducting slab (1cm/a, Cascadia slab, (Hacker et al., 2003). The curve labelled "R & E (2002)" was calculated for a geotherm taken from the numerically modelled exhumation of an exhumed wedge-like sliver of continental crust (Roselle and Engi, 2002).

A 5.2 References for creep parameters

Dry dislocation creep:

Quartzite: Jaoul et al., 1984
Anorthite: Shelton and Tullis, 1981
Olivine: Chopra and Paterson, 1984

Wet dislocation creep:

Quartzite: Jaoul et al., 1984
Wet Diorite: Hansen and Carter, 1982
Olivine: Chopra and Paterson, 1981

Viscous granular flow:

Quartzite: Rutter and Brodie, 2004
Anorthite: Rybacki and Dresen, 2000
Olivine: Handy, 1989

A 5.3 Solid solution endmembers and Margules Parameters

Garnet

Endmembers: Pyrope, Grossular, Almandine, Spessartine

Ideal 1-site-mixing and Margules-type excess function:

Solid solution models:

(1) Ganguly et al. (1996)

Clinopyroxene

Endmembers: Diopside, Hedenbergite, Jadeite

Ideal 1-site-mixing and Margules-type excess function.

Solid solution model: Meyre et al. (1997)

Sodic amphibole

Endmembers: Glaucophane, Fe-Glaucophane

Ideal 1-site-mixing and Margules-type excess function:

Glaucophane-Fe-Glaucophane	W^H	W^S	W^V
112	10000	0.00	0.00

Phengite

Endmembers: Muscovite, Celadonite, Fe-Celadonite; Pyrophyllite

Ideal 1-site-mixing and Margules-type excess function:

modified from Vidal & Parra (2000)

Muscovite-Celadonite	W^H	W^S	W^V
112	-10500.0	55.0	0.79
Muscovite - Fe-celadonite			
112	-10500.0	15.0	0.78
Muscovite - Pyrophyllite			
112	30000.0	20.0	-0.17
122	30000.0	20.0	-0.17

Chlorite

Two different solution models were tested; we preferred the modified Vidal & Parra (2000) model.

Endmembers: Amesite, Clinochlore, Daphnite, Mn-Chlorite.

Ideal 3-site-mixing and Margules-type excess function:

(1) Modified from Vidal & Parra (2000)			
Amesite - Clinochlore	W^H	W^S	W^V
112	-9400	-30	-0.2
Amesite - Daphnite			
112	-12000	35	-0.5
Mn-chlorite - Daphnite			
112	-10000	0	0

(2) Modified from Holland & Powell (1998)			
Amesite - Clinochlore	W^H	W^S	W^V
112	18000	0	0
Amesite - Daphnite			
112	13500	0	0
Clinochlore - Daphnite			
112	2500	0	0

Calcic Amphibole

Endmembers: Pargasite, Fe-Pargasite, Tremolite, Tschermakite, Fe-Tschermakite, Ferro-actinolite

Ideal 3-site-mixing and Margules-type excess function:

modified from Mader et al. (1994)			
Pargasite - Tremolite	W^H	W^S	W^V
112	9743.68	0	0
Tremolite – Ferro-actinolite			
112	2108.23	0	0
Tschermakite - Tremolite			
112	21431.32	0	0
Fe-Tschermakite – Ferro-actinolite			
112	-15492.29	0	0
Tschermakite - Fe-Tschermakite			
112	2108.23	0	0
Pargasite - Fe-Pargasite			
112	2108.23	0	0

Biotite

Endmembers: Phlogopite, Eastonite, Annite, ordered Biotite

Ideal 3-site-mixing and Margules-type excess function:

Phlogopite - Annite	W^H	W^S	W^V
112	9000.0	0	0
Phlogopite - Eastonite			
112	10000	0	0
Phlogopite – o-Biotite			
112	3000	0	0
Annite - Eastonite			
112	-1000	0	0
Annite – o-Biotite			
112	6000	0	0
Eastonite – o-Biotite			
112	10000	0	0

Feldspar

Endmembers: Albite, Anorthite, K-Feldspar

Ideal 1-site-mixing and Margules-type excess function.

Solid solution model: Furman & Lindsley (1988).

A 6 Appendix for Chapter 6

A 6.1 Calculation routine

The algorithm of THERIAK calculates the stable mineral assemblage by minimising the Gibbs free energy (G) in a multicomponent system with fixed bulk rock composition. This is done by several steps including linear and non-linear programming problems. In the first step THERIAK searches each solution phase for the composition with the lowest Gibbs energy of formation ($\Delta_f G$) in the system. The solid solution phases are defined by endmembers, i.e. each solution is considered to be made of any number of species, where each of these species is a valid endmember. $\Delta_f G$ of the solid solutions is defined by the Gibbs-Duhem equation:

$$\Delta_f G = \sum_{j=1}^{ne} x_j \cdot \mu_j ,$$

with:

ne = number of endmembers in the solution phase

μ_j = chemical potential of endmember *j* in the solution phase

x_j = concentration of endmember *j* in the solution phase

and $\mu_j = \mu_j^0 + \alpha \cdot R \cdot T \cdot \ln(a_j)$

where

μ_j^0 = chemical potential of pure endmember j

α = site occupancy integer

R = Gas constant

T = temperature and

a_j = activity of component j in the solution phase.

The solid solution models and Margules parameters used to determine $\Delta_f G$ are given in the Appendix 2. The compositions with the smallest $\Delta_f G$ are added to the database as phases with fixed composition.

In the second step THERIAK determines the mineral assemblage with the lowest Gibbs free energy. This problem can be formulated as:

minimise $G = \sum_{k=1}^{N} n_k \cdot g_k$,

where n_k is the number of moles, g_k is the molar Gibbs free energy of phase k and N is the number of coexisting phases in the system. Details of the algorithm are described in de Capitani and Brown (1987).

A 6.2 Calculation procedure for diffusion controlled garnet growth

Modelling diffusion-controlled garnet growth with the method described above requires that at least one element of the garnet solid solution is independent from the global equilibrium. To model this condition we replaced an endmember of the garnet solid solution, with one that has the same thermodynamic properties as the replaced endmember, but is defined by a substitute element (SE), that is not incorporated into other phases in the system. The thermodynamic implications of that model are displayed by the G-X diagrams in Fig. A 6.1. Three G-X binaries are influenced by our constraints. In the binary between SE and the replaced element (RE), all phases are endmembers, garnet and the SE-oxide being the only phases with a SE-endmember. In the binaries between SE and any other element (Y), garnet forms a solid solution and all other minerals are endmembers. In the binaries between RE and all other elements (Y), garnet is an endmember phase of Y, whereas other phases (A and B) may form solid solutions. The tangent points of the shaded planes to the G-X curves in Fig. A 6.1, that display possible hyperplanes, calculated by the THERIAK-DOMINO algorithm, represent the stable mineral assemblages.

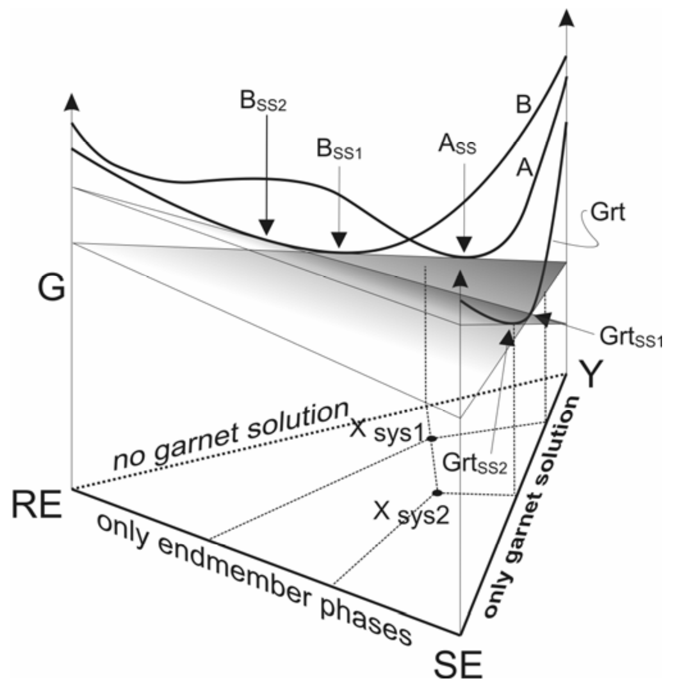

Fig. A 6.1: G-X relations in the binaries *replaced elements-substitute elements-all other elements* (RE-SE-Y). The curved lines display the G-X curves of different minerals (A, B and Grt). The shaded planes display possible hyperplanes that define the mineral assemblage with the lowest Gibbs free energy. Note that changing amounts of SE in the system changes the tangent point of the hyperplane to the G-X curve of garnet and therefore influences the phase relations along other binaries, as displayed by the second, more steeply dipping plane.

In case of the bulk rock composition X_{sys1} the stable assemblage is B_{ss1}+A_{ss}+Grt_{ss1}. Changing amounts of SE in the system, e.g. due to fractional garnet crystallisation or insufficient nutrient supply, may have consequences for phases not containing SE because the tangent point of the hyperplane to the garnet solid solution changes and the new hyperplane might not touch the G-X curves of phase A or B, as demonstrated by the second, more steeply dipping plane, that represents the stable phases for bulk rock composition X_{sys2}. In this case, the stable assemblage is B_{ss2}+Grt_{ss2}. In a multicomponent system $\Delta_f G$ and the components define a hyperspace and the mineral assemblage with the lowest $\Delta_f G$ is defined by a hyperplane that is tangent to the $\Delta_f G$ curves of the (stable) phases.

A 6.3 Solid solution endmembers and Margules Parameters

Garnet

In the models we used the solid solution formulation of Ganguly et al. 1996. A comparison of the results with those calculated with the Berman 1990 formulation showed no significant differences in the garnet zonation patterns.

Endmembers: Pyrope, Grossular, Almandine, Spessartine

Ideal 1-site-mixing and Margules-type excess function:

Solid solution models:

(1) Ganguly et al. (1996)

(2) Berman (1990)

Clinopyroxene

Endmembers: Diopside, Hedenbergite, Jadeite

Ideal 1-site-mixing and Margules-type excess function.

Solid solution model: Meyre et al. (1997)

Sodic amphibole

Endmembers: Glaucophane, Fe-Glaucophane

Ideal 1-site-mixing and Margules-type excess function:

Glaucophane-Fe-Glaucophane	W^H	W^S	W^V
112	10000	0.00	0.00

Phengite

Endmembers: Muscovite, Celadonite, Fe-Celadonite; Pyrophyllite

Ideal 1-site-mixing and Margules-type excess function:

modified from Vidal & Parra (2000)			
Muscovite-Celadonite	W^H	W^S	W^V
112	-10500.0	55.0	0.79
Muscovite - Fe-celadonite			
112	-10500.0	15.0	0.78
Muscovite - Pyrophyllite			
112	30000.0	20.0	-0.17
122	30000.0	20.0	-0.17

Chlorite

Two different solution models were tested; we preferred the modified Vidal & Parra (2000) model.

Endmembers: Amesite, Clinochlore, Daphnite, Mn-Chlorite.

Ideal 3-site-mixing and Margules-type excess function:

(1) Modified from Vidal & Parra (2000)			
Amesite - Clinochlore	W^H	W^S	W^V
112	-9400	-30	-0.2
Amesite - Daphnite			
112	-12000	35	-0.5
Mn-chlorite - Daphnite			

112	-10000	0	0

(2) Modified from Holland & Powell (1998)			
Amesite - Clinochlore	W^H	W^S	W^V
112	18000	0	0
Amesite - Daphnite			
112	13500	0	0
Clinochlore - Daphnite			
112	2500	0	0

Calcic Amphibole

Endmembers: Pargasite, Fe-Pargasite, Tremolite, Tschermakite, Fe-Tschermakite, Ferro-actinolite

Ideal 3-site-mixing and Margules-type excess function:

modified from Mader et al. (1994)			
Pargasite - Tremolite	W^H	W^S	W^V
112	9743.68	0	0
Tremolite – Ferro-actinolite			
112	2108.23	0	0
Tschermakite - Tremolite			
112	21431.32	0	0
Fe-Tschermakite – Ferro-actinolite			
112	-15492.29	0	0
Tschermakite - Fe-Tschermakite			
112	2108.23	0	0
Pargasite - Fe-Pargasite			
112	2108.23	0	0

Biotite

Endmembers: Phlogopite, Eastonite, Annite, ordered Biotite

Ideal 3-site-mixing and Margules-type excess function:

Phlogopite - Annite	W^H	W^S	W^V
112	9000.0	0	0
Phlogopite - Eastonite			
112	10000	0	0
Phlogopite – o-Biotite			
112	3000	0	0
Annite - Eastonite			
112	-1000	0	0
Annite – o-Biotite			
112	6000	0	0
Eastonite – o-Biotite			
112	10000	0	0

Feldspar

Endmembers: Albite, Anorthite, K-Feldspar

Ideal 1-site-mixing and Margules-type excess function.

Solid solution model: Furman & Lindsley (1988).